Reply to the reviewers' comments TC-2015-143 Jansen et al. (Small-scale disturbances in the stratigraphy of the NEEM ice core: observations and numerical model simulations)

We would like to thank the reviewers for their very useful and constructive comments and are delighted to hear that both reviewers recommended publication of our manuscript after the suggested revisions. In the following we state all changes made to the manuscript and give a point-by-point reply to all concerns raised. The reviewer's comments are in black, our replies in blue. We also attached an updated manuscript with highlighted changes as a supplement to an additional post.

Reply to anonymous Referee #1:

The paper is interesting and important, and should be published. The data are fascinating, and the modeling provides insights.
However, I believe that additional issues should be addressed, and that the terminology should be considered more carefully. Terminology is not the most important issue, but I will start with the question of whether these features should be called "kink bands". This is a matter of convention and does not control the physics. However, I strongly advise against calling these "kink bands". The authors provide the quote "Kink-bands [...] can be expected to form in any statistically homogeneous rock which has a high degree of anisotropy and which is compressed in a direction parallel to the foliation" (Cobbold et al., 1971)." Most workers would immediately identify the layering in ice as the dominant foliation. Over time, there is stretching along that foliation and compression perpendicular to it, exactly reversed from the usual expectation of kink bands. The original usage of "kink band" in Orowan (1942) was for features formed in single-crystal compression parallel to the glide plane, but the features here originate almost perpendicular to the mean dominant glide planes of the crystals. Analog experiments have included workers generating kink bands in decks of cards by squeezing along the cards rather than perpendicular to them. (The Orowan, 1942, Nature paper (no. 3788, p. 643) is fascinating, and does include a hypothetical kink band with stress applied at 45 degrees to the glide planes as well as the observed bands with stress parallel to the glide planes.). The authors go on to state "When compressed parallel to foliation, the initial inclination of the kink bands is 45 degrees relative to the foliation. The ELLE model results show a similar feature: for the single maximum fabric vertical stripes develop in the first deformation stages, which only show a slight deviation of the c-axis from the vertical orientation." With the foliation horizontal, the ELLE model results start with near-vertical bands, not at 45 degrees as expected for kink bands. Furthermore, most definitions of kink bands note their tendency to occur in conjugate pairs, but the features in the ice cores do not form conjugate pairs, instead always having the same sense relative to the shear field. Using "kink band" for these features is highly likely to give most readers an initial idea about formation processes that is wrong. The definition of "kink band" as used in the full literature is sufficiently broad that one cannot absolutely insist that the usage here is wrong. But, the usage here is misleading, and should be avoided.

We agree that the paragraph explaining the kinking process was unclear in the first version of the manuscript and led to confusion, as indeed the initial orientation of the kink band is not at 45°, but at 90° to the foliation. It is in fact initially 45° to the maximum compressional stress. We rewrote parts of this paragraph to avoid misunderstanding. We omitted the Cobbold (1971) citation, as it gave the wrong impression that we are looking at a stress regime compressive perpendicular to the foliation. In our case, the foliation of the material is given

by the basal planes of the initial single maximum fabric of the ice crystals, and the deformation is simple shear parallel to these planes.
The comments by the reviewer made it clear to us that we should have clarified better the two mechanisms of kink folding as described by Dewey (1965) in his extensive review of the formation of kink folds (p. 491):
" The first is produced by the development of kink-bands parallel to conjugate planes of maximum shearing stress (dihedral angle < 90”). [...] The second type of conjugate system arises as a direct result of bend gliding. Orowan (1942) and Barrett (1952) have demonstrated the importance of kinking in compressed metals where the plane of gliding is oriented parallel or sub-parallel to 01, i.e., initially parallel to the plane of vanishing shear stress. Barrett showed that kink-planes originate normal to the plane of gliding after elastic distortion ..."
In the idealised second mechanism, deformation is accommodated by "bend gliding", or "flexural slip" in geology. That is slip only parallel to the foliation as a single slip system. As there is zero strain rate perpendicular to the foliation (no thinning or thickening), the banding plane must be the bisector of the interlimb angle, and hence 90° to the foliation at the initiation of kink band formation. In case of foliation-parallel compression (most models and experiments), this second mechanism is inefficient to produce layer parallel shortening, as the kink bands would be perpendicular to sigma1. Conjugate kink bands develop with angles typically 45-70° to sigma1.
Simple shear parallel to the foliation is a special case where the preferred initial orientations for the kink bands of both mechanisms coincide: 90° to the foliation is also the orientation with the greatest effective shear stress. The two mechanisms effectively merge into one. One orientation of the conjugate set is parallel to the foliation and is therefore "invisible". The second orientation is at 90° to the foliation, which - if perfect - would neither stretch nor shorten. Small perturbations lead to kink folds in the foliation, with the foliation rotated in opposite directions in opposite limbs. However, only the rotation that is synthetic with the applied shear will amplify by the overall imposed simple shear, resulting in the kink bands that rotate synthetically with the shear, while simultaneously increasing the angle between the foliation (basal plane) in the kink band and its surroundings. Such kink bands that initially form at a high angle to the foliation have recently been reproduced experimentally by Misra and Burg (2012, Mechanics of kink-bands during torsion deformation of muscovite aggregate, Tectonophysics, reference added to the manuscript).
We thus regard our explanation for near-vertical kink band formation consistent with the Orowan (1942) reference suggested by the reviewer. In his fig. 5 Orowan illustrates the development of kink-bands for oblique foliation under compression and tension, which is an approximate analogue to simple shear parallel to the foliation. in this case the original orientation of the Kink band would be near-perpendicular to the foliation.
In summary, we still do think that it is legitimate to use the term “kink band” for the observational results as well as for the modelled features, and that this is consistent with the literature. We agree however that the Cobbold (1971) citation at the beginning of section 4.2 may have been somewhat misleading and rephrased the beginning of the paragraph to better explain the process of kinking in simple shear.

Moving to more interesting issues, the modeling uses simple shear only. This is fine as a starting point, but is certainly wrong. The authors are correct that basal shear increases downward and layer thinning decreases, but the folds very clearly form at a depth where layer thinning is significant. Stronger wording is needed that the experiments may generate hypotheses but cannot truly test them because stresses and strain rates are omitted that may be important.

At the moment it is not possible to combine pure and simple shear in the ELLE- FFT-simulations. We added a paragraph to the model description, giving more emphasis on the fact that the model setup is a simplified approximation of the real conditions. In the model results section 3.3 we again explain that in the deeper parts of ice sheet the deformation is dominated by simple shear, and our model is an approximation. However, we are confident that the shearing component in combination with the strong fabric is the essential factor for the nucleation and development of the kink bands. The influence of the vertical thinning under real ice sheet conditions may lead to an accelerated tilting of the kink bands due to layer thinning, which is explained in the text.
Rasmussen et al. (2013) show that the change in annual layer thickness decreases significantly below 1500 m, where the folds are observed, indicating the relative dominance of the shear component in deformation.

Perhaps more importantly, by enforcing simple shear, the model does not allow the folds to affect the flow at the 10-cm scale. The existence of a "stripe" of differently oriented grains in a small volume must affect the stresses or the strain rates nearby, and likely both, because of the flow response to the differences in c-axis fabric and possibly other important factors. In turn, if simple shear were to exist far from a stripe, the deformation near the stripe likely would have additional components, and as suggested by Alley et al. (1997), these components might contribute to growth of the folds and perhaps to larger-scale deformation. This limitation should be noted more explicitly; many processes that may be important to fold behavior are not allowed in the modeling.

We do mostly agree with the reviewer here, except the supposition that our model would not allow folds to affect flow on the 10-cm scale. The Full-Field Theory (FFT) model does calculate the full stress and strain rate field and, although the bulk shear strain rate is given, variations in the flow field do develop as a result of the formation of kink bands. Location, spacing and orientation of shear bands are not imposed in the model, but emerge from the small random perturbations in the initial lattice orientations of grains. These influence the strain rate and stress in their neighbourhood, leading to connected zones with rotated orientations of the basal plane: the kink bands or stripes. The Fig S3 is added to illustrate this process.
The objective of this study is to analyse the formation of these structures at the "hand specimen" scale and not at the large (km-) scale, where very likely additional parameters play a role, which are beyond of the scope of the microstructural model. To model larger-scale folds, the length scale and or resolution in the numerical model had to be changed. It can, for example, be envisaged that on larger scales ensembles of small perturbations form larger-scale folds.
We added a sentence to the summary explicitly mentioning our focus on the small scale.

The authors note that the ELLE simulations cause stripes to form, but do not explain what occurs at the grain-scale level in ELLE. Do the stripes initially arise from the random alignments that occur occasionally in a set-up such as that used? And if so, do interactions among these then strengthen the stripes over time by affecting orientations of grains in a nascent stripe or just beyond the end?
The prior work of Alley et al. (1997) addressed these issues, and found an important role for them and for the third-dimensional interactions that are ignored in the 2-d treatment here. Additional discussion should be added.

The initial orientation of the c-axes of the grains is disturbed with a noise of ±5 degrees. This noise is randomly distributed and does not show any initial vertical alignments. Figure S3 in the supplement to this manuscript shows a random distribution of c-axes. The stripes developing in the model appear to grow in length (i.e. the kink-band propagates along the model from a punctual nucleation). This propagation of the kink-band can be observed from the variation of c-axis orientation of grains along the bands: older segments of the kink-band have grains with their c-axis higher tilted/rotated than c-axis in grains inside younger segments.
We added this observation to the model results and discussion and also discuss findings from Alley et al. 1997 in more detail. We can only speculate on the 3-d nature of these bands, but assume that they are planar features, as stated in the manuscript

The authors state "The later onset of folding in the deeper ice cores shows that higher shear strain is required to produce visible folding due to the higher overburden pressure." Overburden pressure is almost certainly irrelevant, aside from a very small activation-volume effect on deformation; most ice-flow modeling omits overburden pressure entirely and focuses only on the local deviatoric stresses.

We agree that the term "overburden pressure" was an unfortunate choice. What is of relevance for the development of folds visible in the line scan data is the ratio between horizontal shear strain rate and vertical thinning. High vertical thinning rates would lead to a flattening of the structures, which then also prevents overturning. The paragraph has been rewritten, and "overburden pressure" has been replaced with "vertical strain-rates".

The authors state "The mechanism of kinking as a trigger for stratigraphic disturbances has already been suggested by Samyn et al. (2011)." True, but the role of these features as contributors to stratigraphic disturbances was a central theme in earlier work, including Alley et al. (1997), which grew out of the GRIP-GISP2 intercomparison effort and involved coauthor Kipfstuhl (Alley, R.B., A.J. Gow, S.J. Johnsen, J. Kipfstuhl, D.A. Meese and Th. Thorsteinsson. 1995. Comparison of deep ice cores. Nature 373(6513), 393-394). The consistency of shear sense noted in the previous paragraph in the new manuscript also was noted in that 1995 work for the GRIP and GISP2 cores.

We agree that the reference to Alley et al. (1995), should be added to the previous paragraph. The reference to Samyn et al. (2011) was specifically chosen for mentioning the term "kinking" as a trigger for disturbances. In the paper from Alley et al. (1997) kinking was explicitly excluded as a mechanism (see next paragraph). Their observation that the fabric stripes are connected to stratigraphy disturbances is already mentioned in the introduction of the manuscript.

Overall, this work presents important new data, of higher quality than in prior work. The use of ELLE also greatly improves on some parts of prior work, but with the difficulty that the stress state used almost certainly omits important effects. The larger picture of some aspects of their formation, their possible growth and how this might affect fold offset, and their larger role in the ice sheet are not addressed despite their importance.
So, significant revision is required, but the good work surely merits publication.

We added statements describing the limitations of the model to the discussion section. We also pointed out more clearly throughout the manuscript that the simple shear environment is

an approximation to the in situ conditions, but also explain why we think this approximation is justified.

Reply to anonymous Referee #2:

Jansen et al. present linescan data from the NEEM ice core. The internal layers visible with this technique show signs of small scale folding and flow disturbances. They show that, where folds are present, the ice crystal orientations present a strong single maximum with inclined bands of grains where the c-axis orientation deviates from the single maximum. They use the ELLE model to discuss their data.
As noted by the first reviewer, the data are well presented and convincing. However the discussion to generalise their interpretation of the folds makes many assumptions on the stress/strain state in the ice cores (especially the role of vertical compression) which are not supported by the model results where only simple shear is applied. I think the discussion part should be revised. Below are my specific comments.

Page 5819, lines 15-19 :"".... (e.g. Paterson, 1991) and may lead to deformation heterogeneities such as non-uniform thinning". Paterson (1991) discuss the feedback between initial viscosity contrast and fabric development, which makes initially softer ice even softer in simple shear. This process has been modelled by Durand et al., Clim. Past., 2007. This has been discussed for large scale flow, and the results show that it is not because ice is softer that it will thin faster, as this will requires, because of mass conservation, some kind of extrusion flow.

We agree that the non-uniform thinning is a controversial issue and probably only important for very special geometries like, for example, small ice caps or cirque glaciers, where extrusion flow might be possible (Waddington, 2010, Life death and afterlife of the extrusion flow theory, Journal of glaciology, 56(200), 973-996). Instead of the non-uniform thinning, we now give shear localization as an example for the effect of rheological differences.

Page 5819, lines 24-25: "Azuma and Goto-Azuma (1996) concluded from model studies with an anisotropic flow law". Azuma and Goto-Azuma (1996) did not used a flow model, they proposed an anisotropic flow law where stress and strain-rate are not co-linear (i.e. the viscosity is a tensor). With this flow law they show that simple shear stresses can produce vertical strain-rates because of the no-co-linearity. They propose a simple sketch where, because of this effect, a layer submitted to simple shear but with different fabrics could exhibit thinning and thickening leading to boudinage. However there is not flow-model (i.e. solving for momentum and mass conservation) in their application.

We agree, and have added "Azuma and Goto-Azuma (1996) concluded from a proposed anisotropic flow law".

Page 5823, lines 12-16: "Starting with the same initial microstructure, models with two different ratios between dynamic recrystallisation (grain boundary migration and recovery) and viscoplastic deformation were performed: 1 and 10 DRX steps per deformation (FFT) step ...". The difference between the two ratios is not discussed in the results section and we don't know for which set-up the results are given.

All model results shown in the manuscript are calculated using the 10 DRX steps. This means that more dynamic recrystallization is performed per deformation step than in the 1 DRX case. In the run with 1 DRX step the bands appear at the same locations as well, but are less intense. An explanation for this is that grains located in kink bands rotated to harder positions are favoured for survival by DRX, increasing the intensity of these bands during the simulation. We omitted the reference to these runs in the manuscript, to keep it concise. We think it would be beyond the scope of this study to examine the sensitivity to DRX in detail.

Section 3.1: It would be interesting to give an idea of the thickness of the annual layers for the different depths. Are the visible layers annual layers?

The thickness of the annual layers is changing from about 2 cm at 1400m depth to less than 1 cm at 2100 m (Rasmussen et al. 2013), below that dating is difficult due to the large scale disturbances (Neem community, 2013). Thus, at least in the undisturbed layers in fig. 1 a the alternating cloudy and clear bands are in the order of the annual layering. We added this to the text in section 3.1.

Section 3.1: When the authors discuss features in the Figures (especially Figure 2), they should put some symbols on the Figure to avoid any ambiguity on which feature is discussed (e.g. line 24 “central greyish layer”).

We have included a symbol indicating the “central greyish layer” and other features in fig.2.

Page 5825, Line 2: “...been flattened out by shear deformation.”. If it is simple shear it should not produce any thinning of thickening?
In this case we did not describe a layer thinning, but a distortion of an overturned fold, in which limbs can become near-horizontal again due to ongoing shear. We rephrased the sentence to clarify this. Thickening or thinning in simple shear depends on the localization of deformation and layer orientation with respect to the shear plane. If simple shear deformation is heterogeneous, there is localization of deformation and therefore thickening or thinning can occur.

Figure 4. Red lines should be thicker to make them more visible.

We have changed red lines to be thicker in fig.4.

Page 5827, lines 9-10 : “This approach is reasonable, since there is a non-coaxial flow component in the region (NEEM Community Members, 2013).” I don't understand the term co-axial here?

Co-axial refers to pure shear deformation (zero internal vorticity) where there is no rotation of the incremental strain axes from an initial to final strain state. Non-coaxial flow refers to cases, including simple shear deformation, where the principal strain axes rotate relative to material lines and therefore do not represent the same material lines with progressive strain (internal vorticity). To avoid confusion we rephrased the sentence.

Page 5828, lines 10-13: “The development of the kink bands is represented in the model run, but the flattening of the structures probably takes place faster under real conditions due to the additional vertical flattening caused by the overlying ice column.” This is not clear. Do the authors assume that there is differential thinning? Or that the bands rotate faster because of compression. Is it not possible to test this with the model and apply both simple shear and

compression?

A mentioned before in reply to reviewer 1, it is unfortunately not yet possible to combine pure and simple shear in an Elle simulation. Thus we make the assumption of simple shear boundary conditions, and justify the approximation by the fact that the observed kink bands occur in a depth dominated by simple shear deformation. We assume that in natural conditions the bands may rotate faster because of the vertical strain rate, which is small but not zero. The thinning of layers does not favor the nucleation of bands, but contributes to their inclination change over time. We rephrased the sentence to better explain the relation.

Page 5829, line 14: "the evolution of an anisotropic fabric (red line) for several ice cores". Not clear how the position of the red line has been chosen. In many cores the development of the fabrics is continuous, so that is it very difficult to give a threshold to define a "single maximum fabric" (caption Fig.10).

In case of the NEEM and the EDML ice cores there is a relative abrupt change in the fabric. For the other cores a depth is used where the eigenvalue reaches a plateau or the displayed data in the literature display a single maximum. The values are based on the literature cited in the caption of figure 10 and in the text. We added a sentence to the text explaining this, and also two more references.

Page 5829, line 17: "Greenland reveal that the onset of visible folding is dependent on the relation between vertical strain rates and shear strain rates (Fig. 10)." Not clear as no indication has been given on this ratio for the different cores. Maybe the depth at witch vertical strain-rates and shear strain-rates becomes equivalent could be evaluated following Montagnat et al., 2014b?

Yes, this is a good point. In the case of the three ice cores (NEEM GRIP and NGRIP) displayed in Montagnat et al. (2014b) the folds begin at the depth where the dominating strain rate changes from vertical to shear, thus at the cross-over of the curves. We added this to the discussion in the text, and discuss the other ice cores in terms of their surface velocity and location (dome, divide, flank). See also the reply to the next comment and related comments of reviewer 1.

Page 5829, lines 21-23: "The later onset of folding in the deeper ice cores shows that higher shear strain is required to produce visible folding due to the higher overburden pressure." I don't see the role of the overburden pressure here. I understand that the authors suggest that the amount of shear should be higher if the vertical strain-rates are higher?
However the overburden pressure do not produce strain-rates, only the deviatoric stresses do. A good proxy for the surface vertical strain-rate is the ratio between ice accumulation and thickness, while the shear stress increase with depth and surface slope (at first order). So that ice thickness only is not sufficient to evaluate the ratio between vertical strain and shear strain.

Reviewer 1 also highlighted this problem and we agree, the paragraph on the comparison of the onset of folding in different ice cores has been rewritten.

Section 4.2 kink-bands...: I have difficulties to follow the discussion here as the citation by Cobbold et al. 1971 speaks of compression to explain the formation of the kink bands while only simple shear is applied here with the model. I think the first paragraph should be

reformulated and maybe illustrated by a cartoon to explain the formation of the bands and their orientation.

We agree, this citation was confusing and we did rewrite the paragraph. We did not insert another sketch but think that figure 9 should be sufficient, at least after rewriting the paragraph. See also the reply to reviewer 1.

Page 5831, lines 21-25: “Azuma and Goto-Azuma (1996) suggested that horizontal variation in the single maximum direction could explain heterogeneous layer thinning or thickening of initially horizontal layers, eventually leading to folding.” The authors already show that they are able to produce some small scale folds with their model in simple shear. Because the flow law proposed by Azuma and Goto-Azuma (1996) applies to fabrics and thus polycristals, I think the mechanism was more suggested for larger scale folds (at least the layers should be larger than a polycristal). So I think this do not apply here.

Azuma and Goto-Azuma mentioned that the horizontal variations in the single maximum could lead to folding, but without mentioning a mechanism providing these initial variations. The kinking we describe in this manuscript could be one possible mechanism providing these. We did rewrite the paragraph to better explain this. The Elle simulations are simulating deformation of a polycrystal, with a very narrow variation in original orientations of the single crystallites.

Page 5833, line 15, “but the results are in line with findings from ice flow models on the larger scale (Azuma and Goto-Azuma, 1996)”. See previous comments.
See above.

Small-scale disturbances in the stratigraphy of the NEEM ice core: observations and numerical model simulations

D. Jansen[1], M.-G. Llorens[2,1], J. Westhoff[2], F. Steinbach[2,1], S. Kipfstuhl[1], P.D. Bons[2], A. Griera[3], and I. Weikusat[1,2]

[1]{Alfred Wegener Institute Helmholtz Centre for Polar and Marine Research, Bremerhaven, Germany}

[2]{Department of Geosciences, Eberhard Karls University Tübingen, Tübingen, Germany}

[3]{Departament de Geologia, Universitat Autònoma de Barcelona, Cerdanyola del V., Spain}

Correspondence to: D. Jansen (daniela.jansen@awi.de)

Abstract

Disturbances on the centimetre scale in the stratigraphy of the NEEM ice core (North Greenland) can be mapped by an optical line scanner as long as the ice does have a visual layering, such as, for example, cloudy bands. Different focal depths allow, to a certain extent, a three dimensional view of the structures. In this study we present a detailed analysis of the visible folds, discuss their characteristics and frequency and present examples of typical fold structures. We also analyse the structures with regard to the deformation boundary conditions under which they formed. The structures evolve from gentle waves at about 1500 m to overturned z-folds with increasing depth. Occasionally, the folding causes significant thickening of layers. Their similar-fold shape indicates that they are passive features and are probably not initiated by rheology differences between alternating layers. Layering is heavily disturbed and tracing of single layers is no longer possible below a depth of 2160 m. C-axes orientation distributions for the corresponding core sections were analysed where available in addition to visual stratigraphy. The data show axial-plane parallel strings of grains with c-axis orientations that deviate from that of the matrix, which shows a single-maximum fabric at the depth where the folding occurs.

Numerical modelling of crystal viscoplasticity deformation and dynamic recrystallisation was used to improve the understanding of the formation of the observed structures during deformation. The modelling reproduces the development of bands of grains with a tilted orientation relative to the single maximum fabric of the matrix, and also the associated local deformation. We conclude from these results that the observed folding can be explained by formation of kink bands

1 Introduction

The NEEM (North Greenland Eemian Ice drilling) ice core, located at 77° 27' N 51° 3.6' W in the northwest of Greenland, has been drilled between June 2008 and July 2012. It is located on a topographic ridge, which dips towards the northwest so that the surface velocities on the ice divide have a non-negligible component of along ridge flow of about 6 m a^{-1} (NEEM community members, 2013). In July 2010 the bedrock was reached at 2537.36 m depth. The site has been chosen in order to recover an undisturbed Eem warm-period ice layer. However, it was found later that the ice below 2200 m was heavily disturbed and probably folded on a large scale (NEEM community members, 2013).

Visual stratigraphy of the NEEM ice core revealed folding also on a small scale, with fold amplitudes varying from less than 1 cm to a few decimetres (Samyn et al., 2011). These types of folds occur well above the large scale disturbances reported by the NEEM community members (2013). Similar structures have been found in the lower parts of other deep ice cores (Alley et al., 1997; Thorsteinsson, 1996; Svensson et al., 2005; Faria et al., 2010; Fitzpatrick et al., 2014). Stratigraphy bands are visualized by an indirect light source scattering on surfaces inside the ice, mainly particles and air bubbles / hydrates (Svensson et al., 2005). High impurity content is found in ice that originates from snow accumulated during glacial periods. Changing impurity contents between ice from glacial and interglacial periods have been linked to rheological differences (e.g. Paterson, 1991) and may lead to shear localization in distinct horizontal layers.

Due to their potential influence on the integrity of the climatic record, folds have been subject to modelling studies (e.g. Waddington et al., 2001). Thorsteinsson and Waddington (2002) explored the amplification of small disturbances in the layering of ice cores for isotropic and anisotropic conditions, investigating the potential for the existence of overturned folds near ice sheet centres. Azuma and Goto-Azuma (1996) concluded from their proposed anisotropic

flow law formulation that an inclined single maximum fabric could lead to vertical strain even in simple shear and thus influence the stratigraphy. They also suggested that horizontal variations in the inclinations could then cause alternating thickening and thinning of layers, leading to folding or boudinage in the stratigraphy. However, the initial formation of the disturbances is not fully understood.

Here we present a characterisation of the small-scale folding observed in the NEEM ice core. Another feature occasionally observed along with folding in deep ice cores are "fabric stripes" (Alley et al., 1997). They describe bands of deviating grain orientations with respect to the surrounding matrix, which is essentially a single maximum fabric in regions where folding occurs. We discuss possible folding mechanisms and the link to the so called "Alley-stripes" in the crystal fabric of grains. Microstructural modelling with ELLE reproduces similar fabrics and fold structures to the ones we observe in the NEEM ice core.

2 Methods

The data used in this study were obtained by different observational methods, which will be introduced only briefly in the following section. For technical details we recommend to check the original literature cited in the subsections.

2.1 Linescan visual stratigraphy

The visual stratigraphy of the NEEM ice core was recorded by means of an automated linescan instrument (see Svensson et al. (2005) for a detailed description of the instrument and data from the North GRIP ice core). Clear ice appears dark when illuminated by an indirect light source. Dust particles or bubbles cause scatter of light and make the ice appear bright in the linescan image. A clear correlation between backscatter and dust content has been found in the North Grip ice core (Svensson et al., 2005). The method can be applied directly in the field and in the case of the NEEM ice core was applied continuously for the entire core, with a gap between 860 m and 1150 m, which corresponds to the brittle zone where the core quality did not allow preparation for the linescanner. For the NEEM ice core the linescan images were recorded with a standardised exposure time and three focal planes within the ice core section with a vertical distance of 1 cm (Kipfstuhl, 2010). This allows to a certain degree a three-dimensional mapping of the visible layering in the ice core. The data are stored in high-resolution (118 pixel per centimetre) bmp images. One drawback of this

method is, of course, that it only shows disturbances in the ice if scattering surfaces are included. However, it is possible to even reveal structures at low dust content by means of image processing and filtering.

2.2 Automated Fabric Analyzer

The crystal fabric orientation of discrete samples was measured using a G50 Automatic Fabric Analyzer (Australian *Russell-Head* type, see e.g. Russell-Head and Wilson, 2001; Peternell et al., 2010, data set: Weikusat and Kipfstuhl, 2010). Samples cut from the physical properties part of the NEEM core were cut to 250 µm thin sections to measure c-axis crystal lattice orientations by polarized light microscopy, where the thin section is placed between systematically varying crossed polarizers (e.g. Wilson and Russell-Head, 2003). The data coverage is much better than in previous ice cores with continuous sampling of selected core sections (bags) to investigate meter-scale variations in fabric throughout the core. However, due to the time-consuming preparation of the samples it was not possible to produce a continuous record.

2.3 Microstructural modelling with ELLE and full field crystal plasticity

We use 2-D numerical modelling to investigate the development of strain localization in a polycrystalline aggregate. At the moment it is not possible to combine simple shear and pure shear boundary conditions. We chose simple shear boundary conditions as an approximation for the in-situ conditions in the lower part of the ice shelf where the fabric stripes are observed, and where horizontal shear is dominant. The simulation approach couples a full field method based on the fast Fourier transform (FFT) that simulates viscoplastic deformation, with a front-tracking codes that simulate dynamic recrystallisation processes (DRX), included within the open-source numerical modelling platform ELLE (http://www.elle.ws; Bons et al., 2008). ELLE has been successfully used to simulate evolution of microstructures during deformation, such as recrystallization (Piazolo et al., 2008; Roessiger et al., 2011; 2014) or strain localisation (Jessell et al., 2005; Griera et al., 2011, 2013). The full-field crystal plasticity (FFT) code (Lebensohn, 2001; Lebensohn et al., 2008; Montagnat et al., 2014a) simulates deformation by pure viscoplastic dislocation glide. An experimental run consists of iterative applications of small increments ($\Delta\gamma$=0.04) of simple shear deformation, each followed by a sub-loop of processes simulating dynamic recrystallisation (grain boundary migration and recovery). While grain boundary migration

123 covers the motion of high-angle grain boundaries, recovery achieves a decrease in
124 intracrystalline heterogeneities by means of local rotation without motion of high-angle
125 boundaries. The recrystallisation sub-loop may be called more than once to simulate the
126 different balance between deformation and recrystallisation as a function of strain rate, since
127 all simulations are performed with the same intrinsic mobility value (M_0) and boundary-
128 diffusion activation energy (Q) (Roessiger et al., 2014; Llorens et al., in review). Exchange of
129 data between ELLE and FFT is possible, as both use periodic boundary conditions and the
130 physical space is discretised into a shared regular node mesh.

131

132 The ELLE data structure consists of three layers: (1) a network of nodes (boundary nodes or
133 *bnodes*) that are connected by straight boundary segments that define the high-angle grain
134 boundaries that enclose individual ice grains, (2) a set of unconnected nodes (*unodes*) to map
135 lattice orientations and dislocation densities, used for the FFT calculation, and (3) a passive
136 marker grid utilised to track finite strain. Distances between nodes are kept between 5.5×10^{-3}
137 and 2.5×10^{-3} times the unit distance (in a 1x1 bounding box), by removing *bnodes* when their
138 neighbours are too close or adding *bnodes* when two nodes are too far apart. The space is
139 discretised in a mesh of 256x256 Fourier points, resulting in a unit cell defined by 65,536
140 discrete nodes. Each *unode* represents a small area or crystallite with a certain lattice
141 orientation, defined by Euler angles, and a dislocation density value. The ELLE data structure
142 has fully wrapping boundaries. The 10x10 cm^2 initial microstructure has 1632 grains, each
143 with a homogeneous lattice orientation, showing a c-axis preferred orientation almost
144 perpendicular to the shear plane, in order to simulate an intrinsic anisotropic material. The
145 misorientation between grains was set at <5º (i.e. initial noise). Dislocation glide of ice-single
146 crystal was defined by slip on the basal {0001}{11-20}, prismatic {1-100}{11-20} and
147 pyramidal systems {11-22}{11-23}. In these simulations, the ratio A of critical resolved shear
148 stress (CRSS) for non-basal versus basal slip systems was set to A = 20. The same stress
149 exponent (n = 3) is set for all slip systems. The physical values used for recrystallisation are:
150 intrinsic mobility M_0 (0.023 $m^2kg^{-1}s$; Nasello et al., 2005), boundary-diffusion activation
151 energy Q (40 KJ mol^{-1}; Thorsteinsson, 2002), isotropic surface energy γ_e (0.065 Jm^{-2};
152 Ketcham and Hobbs, 1969) and temperature was set to T=-30ºC. To simulate recovery
153 numerically, a modification of the approach proposed by Borthwick et al. (2013) was used.
154 As the time step for the simulation of recrystallisation is smaller than necessary for the

155 computationally expensive FFT-calculation, we modelled ten DRX steps of Δt=6.3x10^{8} s for
156 each shear strain increment of $\Delta\gamma$=0.04, giving a shear strain rate of 6.35x10^{-12} s^{-1}.
157 Simulations with other shear strain rates were performed for comparison, but not presented
158 here. See Llorens et al. (in review) for a complete description of the methods.

159

160 # 3 Results

161 ## 3.1 Stratigraphy and fold classification

162 The stratigraphic data were visually inspected for all parts of the ice core containing cloudy
163 bands, in order to categorise disturbances of the visible layers. It has to be noted that this
164 method is only appropriate where sufficient layers are visible, since clear ice may have been
165 deformed as well. Figure 1 shows an overview of the layering structures we find in the NEEM
166 ice core. All images shown are confined to the core sections above the major disturbances in
167 the Eemian ice beginning at a depth of approximately 2200 m. Around this depth the ice is
168 heavily sheared and the layering becomes more and more diffuse. Below that it is no longer
169 possible to see fold structures in the visual stratigraphy data as the ice of the Eemian is mostly
170 clear . The panels display the scans of entire core sections of about 1.10 m, which were cut
171 into segments of 0.55 m after scanning. The top always represents the upper part of the core
172 segment. Some segments differ in length, as the recovered core pieces are not always exactly
173 1.10 m long. Some of the pieces also fractured during the recovery process or during
174 preparation, which is highlighted with red lines in figure 1. The images have been partly
175 processed by applying a Gauss filter to enhance the visibility of the layering, and therefore the
176 grey values are no absolute measure for impurity content or of other parameters that could
177 influence the backscatter within the ice.

178 The upper part of the NEEM ice core shows little or no disturbances. Figure 1a shows an
179 example from 1430 m depth with perfectly horizontal layers. The layer thickness and opacity
180 does vary in the core segment, and single layers have a constant thickness throughout the 10
181 cm wide core section. A close up of one of the layers shows no particular structure within it
182 (fig. 2a). According to the NEEM chronology published in Rasmussen et al. (2013), the
183 annual layer thickness changes from about 2 cm at 1500 m to less than 1 cm at 2000 m depth.
184 Below a depth of about 1700 m the structure of the layering begins to change, as examples
185 from depths of approximately 1760 m and 1867 m show (fig. 1b,c). Wave-like features with

cm-scale amplitudes and wavelengths in the order of the core diameter can be observed. In some parts of the core segments these disturbances can be clearly followed through several layers. Figure 2b shows an enlarged section of figure 1b, showing a well-developed asymmetric z-fold. Its shape indicates sinistral shear and the fold is beginning to overturn. The fold hinge is a sharp feature, which can be followed over several layers. The enlargements in figure 2b also show that the cloudy layers themselves appear to be laminated.

For the core sections shown in figure 1b,c the layers vary in thickness within the core, as can be clearly seen in figure 2b, where the central greyish layer (indicated with green dashed lines) nearly doubles its thickness in the centre of the image due to the folding. This shape is typical for so-called similar folds in geology (Ramsey et al., 1987). Figure 1d,e show examples from 1977 m and 2098 m depth, where the layering is significantly more disturbed. The vertical scale of the disturbances has risen to the scale of ten centimetres (fig. 2d,e). In between the larger-scale folds the layering appears to be more regular again, however the limited width of the core sections limits our interpretation here, as the layers could be overturned folds of which the limbs became near-horizontal due to a combination of the on-going shear and vertical thinning. Figure 2c shows a stack of flattened folds, where the doubling of layers may not be immediately obvious to the observer when focusing on the left part of the image Tracing one boundary between a clear and a cloudy band highlights that the thin layers are probably limbs of an overturned fold (indicated with a blue dashed line). There are also new generations of folds standing out through their well-defined and steeper axial planes and which are not yet overturned (fig. 2c, on the left, fold axis indicated with a green dashed line).

At even greater depth the layering becomes less distinct (fig. 1f,g,h). In some parts of these sections the layers appear to be undisturbed but inclined, which may indicate that they are part of a larger deformation structure. The now very thin layers still show new generations of folds.

3.2 Crystal fabric orientation anomalies connected to folds

In comparison to previous deep ice cores, the amount of data gathered to analyse ice fabric is relatively high. To investigate small-scale variations entire bags of 55 cm from certain depths were processed. The general evolution of ice fabric with depth in the NEEM ice core was described in Montagnat et al. (2014b). The c-axis orientation distribution develops more or

less linearly from an isotropic fabric to a single maximum at a depth of about 1400 m, which represents the transition from the Holocene to the last glacial (Rasmussen et al., 2013). Within the well-developed single maximum fabric we found inclined bands of grains with a deviating c-axis orientation. We assume that the bands are planar features, but as the thin sections are vertical cuts through the cylindrical core section the inclination of the bands is not necessarily equal to the inclination of the planes. Similar bands were described in the GRIP ice core (Thorsteinsson, 1996) and the GISP2 ice core (Alley et al., 1997). In case of the NEEM ice core, however, significantly more fabric data are available, which enables us to follow these structures through entire core sections.

One of the first examples of such a band, shown in figure 3a, appears at a depth of 1800 m. The c-axis orientation of grains within the bands is tilted anti-clockwise relative to the single maximum, which is indicated by the blue-greenish colours in the colour wheel used to illustrate c-axis orientation (inset in figure 3a). The grain size does not differ from the average grain size of the sample. The subgrain boundary density in these grains does not differ significantly from the surrounding ones, which indicates that they are most likely not newly nucleated grains (fig. 4). However, while the subgrain boundaries in grains with vertical c-axes are mostly parallel to the basal planes, they are mainly perpendicular to the basal plane in grains within the band, indicating the onset of rotation recrystallisation.

The direct comparison of the fabric data with the line scan images (figure 3) reveals that these bands are connected with disturbances in the layering. The inclination is in agreement with the sense of shear that is derived from the asymmetry of the folded layers. However, layer disturbances are not always visible where fabric anomalies are found.

In figure 5a,b,c the three linescan images available from the different focal depths are plotted next to each other to illustrate the three-dimensional nature of the observed folding in the layering. The shape change of the highlighted layer indicates that the fold axis shifts to the left towards the centre of the core (fig. 5e). The thin sections for the fabric analysis are prepared from the physical properties sample in the upper part. The linescan measurement is performed on the remaining part of the core with 1 cm between the different focal planes (fig. 5d).

Figure 6 shows an example from approx. 1978 m depth where we see finely laminated layers and asymmetric folds that indicate dextral shear. The fold hinges indicated by the arrows are not very distinct, which is probably due to light diffusion caused by the distorted fine layers.

The two distinct bands in the right half of figure 6a are relatively steep and exhibit a small tilt in the c-axes, while the feature indicated by the central arrow is more flattened and also shows a higher tilt in the c-axes. Another example can be found in the supplementary material (figure S1). Where several bands occur in one core section, their inclination and orientation appears to be consistent throughout (fig. 7).

3.3 Model results

To understand the development of the observed fabric anomalies and the related disturbances in the layering, we simulated the fabric evolution under simple shear with an initially well-developed single maximum orientation distribution. A random noise of <5° was added to grain orientations. The setup of the simulation does not fully represent the probable kinematic boundary conditions in the region of the ice core where we observe the structures, which would be a combination of vertical compression and simple shear (Montagnat et al., 2013). We, however, model these structures in simple shear for simplicity. This approach is reasonable, since there is a significant flow along the ridge of about 6 m a^{-1} (NEEM Community Members, 2013), which gives the core location the character of a flank with relatively high shear strain rates, rather than a divide. Moreover, the choice of simple-shear boundary conditions is also justified by the fact that the bands start to appear in the lower third of the ice sheet where shear stress becomes the dominant driver for deformation (Montagnat et al., 2013). However, there might be aspects of the evolution of the folds that cannot be reproduced due to the simple shear approximation.

In the model simulation vertical bands similar to the ones observed in the ice core begin to stand out after a shear strain of γ = 0.6, but start to appear already after small strains (supplementary material figure S3). In the initial conditions the small deviations of the c-axes from the vertical are randomly distributed and do not show alignment (figure S3 a). During the first deformation steps narrow vertical bands develop with deviations from the single maximum towards the shear direction as well as broader bands with an opposite rotation of the c-axes. The rotation of c-axes in the narrow bands intensifies during the next steps and the bands begin to tilt due to the continuing shear deformation (supplementary material figure S2). The rotation of the c-axes is twice the inclination of the band, which is typical for flexural-slip kink bands (supplementary material figure S4; Dewey, 1965; Tanner, 1989). Figure 8a,b,c shows the c-axis orientations for the sample after shear strains of γ=1, γ=2 and γ=3. The bands seem to develop in different generations, which can be distinguished by their

inclination as the new bands are steeper. There are areas between the bands where orientations of c-axes rotate anti-clockwise (magenta coloured), but on a larger scale and with less well-defined boundaries. In later stages of the simulation the oldest bands begin to disintegrate with the grains recrystallizing back to a vertical c-axis fabric.

Figure 8d,e,f shows the development of a passive marker grid during the simulations. The blue lines were perfectly horizontal at the beginning of the simulation and can be regarded as an analogue to the stratigraphic layering observed in the ice core. It is apparent that the bands with abnormal grain orientation are connected with folding in the layering. At first these disturbances appear as small steps, but they develop into overturned folds with a short and steep limb with progressive deformation. They correspond to the well-developed bands in the fabric, and to a long, less inclined limb, representing the area in between the bands. The disturbances in the layering are permanent, and therefore the bands are visible in the passive grid even when they no longer exist in the orientation plot. The rotation rate of the kink bands in the model run is controlled by the applied overall perfect simple shear deformation. If there is an additional component of vertical shortening, as in a natural ice sheet, the rotation rate is expected to increase.

Figure 8g,h,i shows the equivalent von Mises strain-rate for the deformation steps γ=1, γ=2 and γ=3. The strain-rate appears to be localized around the margins of the bands where bending strain is the highest, which is most apparent for newer bands with steep inclinations. One also sees that strain rate localises in horizontal zones as well, which is not visible in passively deformed horizontal lines (fig. 8d-f).

4 Discussion

4.1 General discussion of folds

The shape of the observed folds in the NEEM ice core is typical for similar folds, as the layers are thickened in the hinge region and thinned in the fold limbs. Similar folds are passive features, where all layers of the package are deformed in a similar way (fig. 9a). They form by passive shearing of the layering and can evolve to become overturned z-folds or even sheath folds (Quinquis et al., 1978; Bons and Urai, 1996; Alsop and Carreras, 2007). Competence or viscosity contrast between the different layers plays no or only a minor role. In contrast, buckle folds (fig. 9b) develop when layers have different viscosities. A competence contrast

312 with a ratio of at least about 25 between strong and weak layers is required to develop distinct
313 folds (Llorens et al., 2013a,b). When a stack of strong and weak layers is shortened, the
314 strong layers form folds by bending, which suppresses thickening or thinning of these layers.
315 The weak layers accommodate this bending by ductile flow into the hinge regions, a process
316 known as flexural flow (Donath and Parker, 1964). Strong and weak layers are thus different
317 in shape (fig. 9b). The folding shapes observed in the NEEM core, however, appears to be
318 consistent in a stack of several layers (figs.1 and 2), which indicates that viscosity contrast are
319 very low and the folds formed by passive shearing, although there may be differences in the
320 flow strength of the ice between the layers due to different impurity content (Paterson, 1991).

321 Figure 10 gives an overview of the onset of folding (black line) and the evolution of an
322 anisotropic fabric (red line) for several ice cores. Comparison with data from EDML (Faria et
323 al., 2010) and WAIS (Fitzpatrick et al., 2014) in Antarctica and with GRIP (Thorsteinsson,
324 1996), GISP2 (Alley et al., 1997; Gow et al., 1997) and North GRIP (Svensson et al., 2005;
325 Wang et al., 2006) from Greenland reveal that the onset of visible folding is dependent on the
326 relation between vertical strain rates (shortening) and shear strain rates (figure 10). Due to the
327 high vertical strain rates, fold structures are flattened out before they overturn, and are thus no
328 longer visible. This has been theoretically described by Waddington (2001). Thus, the
329 dynamical setting of the borehole location is, in addition to the anisotropy, an essential
330 parameter for the onset of visible folding. An ice core at flanks or on divides with non-
331 negligible flow along the ridge, samples ice which experiences more shear strain than an ice
332 core at dome positions. While the GISP 2 and North GRIP ice cores are very similar in ice
333 thickness and accumulation rate to GRIP, the onset of folding for the latter is 300 m deeper,
334 which may be due to its dome position and the lower surface velocity (for a comparison of ice
335 core parameters see Faria et al. (2014)). In the region of the NEEM ice core there is an even
336 higher along-ridge flow. A comparison of shear strain rates profiles with depth at the NEEM,
337 GRIP and North GRIP locations can be found in Montagnat et al. (2014b). The depths of the
338 crossing points of the curves for shear and vertical strain rates that is displayed in Montagnat
339 et al. (2014b) corresponds approximately to the onset of folding in the cores.

340 The EDML ice core stands out in the comparison shown in figure 10, as the folding begins
341 significantly higher than the establishment of a single maximum fabric. However, Faria et al.
342 (2010) report that a strong girdle fabric has formed in the region of the onset of folding, thus
343 the fabric does show some anisotropy there as well.

The scale of the disturbances found in the layering of the NEEM ice core is very similar to the ones observed at EDML (Faria et al., 2010) and North GRIP (Svensson et al., 2005), for both of which a linescan dataset of comparable quality as for the NEEM ice core is available.

The very deep onset of folding in the WAIS ice core might be due to strong basal melting at this site (Fitzpatrick et al., 2014; WAIS Divide Project Members, 2013).

4.2 Kink bands as a source for folding

Ice is a mechanically highly anisotropic mineral, as is polycrystalline ice with a strong single-maximum c-axes distribution. Kinking has been observed in single ice crystals as well as in polycrystalline aggregates under compression (Wilson et al., 1986). Kink bands are also common in well-foliated rocks, which therefore exhibit a strong mechanical anisotropy (REFS). There are basically two mechanisms for the formation of kink bands (Dewey, 1965), which may act in concert. The first is shear localisation, which occurs approximately parallel to the planes that experience the highest net shear stress. The result is a conjugate set of kink bands, originally at a high angle to each other. The second mechanism is a combination of localised bending and flexural slip. There is no thickening or thinning perpendicular to the foliation if the material can only deform by slip parallel to that foliation. A geometric necessity of this type of folding is that the axial plane must be the bisector of the interlimb angle (fig. 9c) (Frank and Stroh, 1952; Dewey, 1965; Cobbold et al., 1971). With the interlimb angle at the beginning of folding being 180°, the kink bands initiate at 90° to the foliation.

Simple shear parallel to a foliation is a special case where the orientations of kink bands formed by both mechanisms is identical: 45° to the maximum compression, which coincides with parallel and perpendicular to the foliation. Foliation-normal kink bands have indeed been observed in simple shear experiments (Misra and Burgh, 2012; Williams and Price, 1990), and developed in our numerical model. Kink bands parallel to the foliation are difficult to observe in natural samples, as these would not fold the foliation. However, the numerical model shows shear-plane parallel localisation of strain rate as well (Fig. g-i).

Kink bands rotate passively, if there is a layer-parallel shear component, which does not necessarily have to be the dominant deformation component. As the kink band rotates by an angle α to the long limb, the short limb has to rotate by 2α, as is observed in the NEEM core and numerical simulations (fig. 8d,e,f). Alley et al. (1997) suggested that the rotation of the c

axes of grains in the stripes lag behind the rotation of the bands themselves, while our model results are following the relation typical for kink bands, with c-axes rotating twice as fast as the axial plane or stripe (supplementary figure S4). Alley et al. 1997 explained the growth in length by the sense of shear at the perimeter of the stripe, which would cause a "spinning" to adjacent grains, causing their c-axes to rotate towards the inclination of the band and thus elongate it. In our numerical model we observe that kink bands are seeded by individual grains and develop by linking these (fig S3). However, their intensification under rotation appears to propagate along their length (fig. S4).

With progressive rotation of the kink bands they become more distinct. Rotation of the short limb occurs by sliding parallel to the basal plane with a sense opposite to the overall shearing direction (fig. 9c). Kink bands finally "lock up" when the interlimb angle reduces to 90°, i.e. when the kink bands are approximately 45° to the layering. In the numerical simulations we see that kink bands begin to disintegrate at this stage, with recrystallization and recovery consuming the grains with deviating orientations and flow homogenizing again (see fig. 8). However, marker lines, such as the layers in the NEEM core, will still record the kink bands, which now continue shearing and develop into passive folds.

In summary, the model results indicate that the evolution of kink bands is a consequence of a fabric with a strong anisotropy with superimposed small random disturbances. In this way grains orientated unfavourably for basal glide are rotated by rigid body rotation and internally reversed shear into a more favourable position in relation to the bulk shear strain. Thus, kinking appears to be an essential process in ice deformation under shear.

Azuma and Goto-Azuma (1996) suggested that horizontal variation in the single maximum direction could explain heterogeneous layer thinning or thickening of initially horizontal layers, eventually leading to folding. The development of kink bands is a process providing such variations in the fabric.

A difficulty in comparing the results of the simulation with the observational data is that with fabric measurements we can only capture a 2-dimensional section of a 3-dimensional feature. Assuming that the kink bands are planar features, the angle at which the cylinder of the ice core is cut relative to the inclination of the plane determines its appearance in the 2-dimensional section. Thus, the inclination of the observed bands in the plane is not sufficient to describe the full orientation of the kink-band plane, but instead gives a minimum

406 inclination of the plane. This also has to be taken into account when interpreting the fold
407 structures on the linescan images.

408 Within one 55cm section of the ice core (bag) the cutting plane through the core is consistent
409 and so are the samples used to prepare the thin sections for the fabric measurements. Figure 7
410 shows that within one bag the inclinations of the kink bands are consistent as well,
411 strengthening the assumption that they are connected to the local stress environment and to
412 the sense of shear, projected onto the plane of the thin section or linescan image. A
413 consistency between the direction of shear and the shape of z-folds in the stratigraphy has
414 been also reported for the GRIP and GISP2 ice cores (Alley et al., 1995). In both examples
415 displayed in figure 7 different generations of kink bands can be detected, differing in
416 inclination of the bands as the older bands have been subjected to more shear strain since their
417 formation, and the corresponding shift in c-axes orientation, as it is seen in the model results
418 as well.

419 The mechanism of kinking as a trigger for stratigraphic disturbances has already been
420 suggested by Samyn et al. (2011). Together with the microstructural model results the
421 observations can be interpreted with an improved understanding of the kinking process. Alley
422 et al. (1997), who described similar bands in the GISP2 ice core, state that the observed bands
423 are most likely not kink bands, as they would require a compressional regime in the horizontal
424 direction. However, the model results clearly show that kink bands can form in simple shear
425 conditions. At the moment it is not clear why the bands sometimes appear dark in the linescan
426 images, but from deeper parts of the core where the crystals are larger in size the linescan
427 images give indication the backscattering can be subject to the crystal orientation.

428

429 ## 5 Summary and conclusions

430 The onset of small-scale folding can be observed at the start of the lower third of the NEEM
431 ice core, which is similar to the fold evolution observed in EDML. Below a depth of about
432 2160 m it is no longer possible to track stratigraphic layers. The shape of the observed
433 structures indicates that they are not buckle folds, which means that they are not originated by
434 a competence contrast between alternating layers. The amounts of folding as well as the state
435 of disturbance increase with depth.

Folding causes thickening of cloudy bands and can potentially influence the resolution of climate data extracted from the NEEM ice core. Folding causing doubling of layers was observed below a depth of about 2100 m. In some core sections the layering appears to be intact in between larger folds in the linescan data. However, within a core section, only folds and doubling of layers up to the scale of 10 cm can be delineated with certainty. It is therefore difficult to ascertain that the climate signal is not disturbed in regions with parallel layering, as these could potentially be part of larger-scale folds.

Microstructural numerical modelling results indicate that the observed folding is initiated by kinking. The onset of kinking requires a highly anisotropic material and thus a well developed single maximum fabric. Local deviations from the single maximum in the direction of shear provide the seeds for kink band development and thus folding. Here we have shown that this process is active on the microstructural scale. Their possible link to larger scale folds still has to be investigated, but could be in line with suggestions by Azuma and Goto-Azuma (1996). Grains with inclined basal plane orientations within the kink bands are eventually eroded through recrystallisation and recovery. However, the kink bands formed folds in material planes that further evolve by passive folding, which is is visible in the layering, but not in the c-axes patterns.

Acknowledgements

This work was carried out as part of the Helmholtz Junior Research group "The effect of deformation mechanisms for ice sheet dynamics" (VH-NG-802). F. Steinbach was funded by the DFG (SPP 1158) grant BO 1776/12-1. The NEEM Linescan data as well as the NEEM fabric data has been made available by www.pangaea.de. The Authors would like to thank Sergio H. Faria and Rüdiger Kilian for helpful discussions. The constructive and supportive comments of two anonymous reviewers and the editor J.-L. Tison helped to significantly improve the initial manuscript. We also would like to thank all members of the NEEM Community who did prepare the physical properties samples in the field.

NEEM is directed and organized by the Center of Ice and Climate at the Niels Bohr Institute and US NSF, Office of Polar Programs. It is supported by funding agencies and institutions in Belgium (FNRS-CFB and FWO), Canada (NRCan/GSC), China (CAS), Denmark (FIST), France (IPEV, CNRS/INSU, CEA and ANR), Germany (AWI), Iceland (RannIs), Japan

(NIPR), Korea (KOPRI), The Netherlands (NWO/ALW), Sweden (VR), Switzerland (SNF), United Kingdom (NERC) and the USA (US NSF, Office of Polar Programs).

References

Alley, R. B., Gow, A. J., Johnsen, S. J., Kipfstuhl, J., Meese, D. A., and Thorsteinsson, Th., 1995. Comparison of deep ice cores. Nature, 373(6513), 393-394.

Alley, R. B., Gow, A. J., Meese, D. A., Fitzpatrick, J. J., Waddington, E. D. and Bolzan, J. F., 1997. Grain-scale processes, folding, and stratigraphic disturbance in the GISP2 ice core. J. Geophys. Res., 102 (C12), 26819-26830.

Alsop, G. I. and Carreras, J. 2007. The structural evolution of sheath folds: A case study from Cap de Creus. J. Structural Geology, 29, 1915-1930. doi:10.1016/j.jsg.2007.09.010.

Azuma, N., and Goto-Azuma, K., 1996. An anisotropic flow law for ice-sheet ice and its implications. Annals of Glaciology, 23, 202-208.

Bons, P. D., and Urai, J. L.,1996. An apparatus to experimentally model the dynamics of ductile shear zones. Tectonophysics 256, 145-164, doi:10.1016/0040-1951(95)00161-1.

Bons, P. D., Koehn, D. and Jessell, M. W., 2008. Lecture notes in earth sciences. In: Bons P. D., Koehn D., Jessell M., editors. Microdynamic Simulation. Springer, Berlin; number 106. 405 pp.

Borthwick, V. E., Piazolo, S., Evans, L., Griera, A. and Bons, P. D., 2013. What happens to deformed rocks after deformation? A refined model for recovery based on numerical simulations. *Geological Society, London, Special Publications, 394*. doi 10.1144/SP394.11.

Cobbold, P. R., Cosgrove, J. W. and Summers, J. M., 1971. Development of internal structures in deformed anisotropic rocks. Tectonophysics, 12: 23-53.

Dewey, J. F., 1965. Nature and origin of kink-bands. Tectonophysics, 1, 459-494.

Donath, F. A., and Parker, R. B., 1964. Folds and folding. Geol. Soc. America Bulletin, 75, 45-62. doi:10.1130/0016-7606(1964)75[45:FAF]2.0.CO;2.

Faria, S. H., Freitag, J. and Kipfstuhl S., 2010. Polar ice structure and the integrity of ice-core paleoclimate records. Quaternary Science Reviews, 29, 338-351.

Faria, S. H., Weikusat, I., and Azuma, N., 2014. The microstructure of polar ice. Part I: Highlights from ice core research. Journal of Structural Geology, 61, 2-20, doi:10.1016/j.jsg.2013.09.010.

Fitzpatrick, J. J., Voigt, D. E., Fegyveresi, J. M., Stevens, N. T., Spencer, M. K., Cole-Dai, J., Alley, R. B., Jardine, G. E., Cravens, E. D., Wilen, L. A., Fudge, T. J. and McConnell, J. R., 2014. Physical Properties of the WAIS Divide ice core, J. Glac., 60 (224), 1181-1198, doi: 10.3189/2014JoG14J100.

Frank, F. C. and Stroh A. N., 1952. On the theory of kinking. Proceedings of the Physical Society (Section B), 65(10), 811-821.

Gow, A. J., Meese, D. A., Alley, R. B., Fitzpatrick, J. J., Anandakrishnan, S., Woods, G. A., and Elder, B.C., 1997. Physical and structural properties of the Greenland Ice Sheet Project 2 ice core: a review. Journal of Geophysical Research, 102 (C12), 26559-26575.

Griera, A., Bons, P. D., Jessell, M. W., Lebensohn, R. A., Evans, L. and Gomez-Rivas, E., 2011. Strain localization and porphyroclast rotation. Geology 39, 275-278.

Griera, A., Llorens, M.-G., Gomez-Rivas, E., Bons, P. D., Jessell, M. W., Evans, L. and Lebensohn, R.A., 2013. Numerical modeling of porphyroclast and porphyroblast rotation in anisotropic rocks. Tectonophysics 587, 4-29.

Jessell, M. W., Siebert, E., Bons, P. D., Evans, L., and Piazolo, S., 2005. A new type of numerical experiment on the spatial and temporal patterns of localization of deformation in a material with a coupling of grain size and rheology. Earth and Planetary Science Letters, 239, 309-326. doi:10.1016/j.epsl.2005.03.030.

Ketcham, W. M., and Hobbs, P. V., 1969. An experimental determination of the surface energies of ice. Philosophical Magazine, 19(162), 1161-1173.

Kipfstuhl, J., 2010. Visual stratigraphy of the NEEM ice core with a linescanner. Alfred Wegener Institute, Helmholtz Center for Polar and Marine Research, Bremerhaven, Unpublished dataset #743062.

Lebensohn, R. A., Montagnat, M., Mansuy, P., Duval, P., Meysonnier, J. and Phillip, A., 2008. Modeling viscoplastic behaviour and heterogeneous intracrystalline deformation of columnar ice polycrystals. Acta Materialia, 57, 1405-1415.

525 Lebensohn, R. A., 2001. N-site modeling of a 3D viscoplastic polycrystal using Fast Fourier
526 Transform. Acta Materialia, 49, 2723-2737.

527 Llorens, M.-G., Griera, A., Bons, P. D., Roessiger, J., Lebensohn, R. and Weikusat, I., in
528 press. Dynamic recrystallization of ice aggregates during co-axial viscoplastic
529 deformation: a numerical approach. Journal of Glaciology, doi: 10.1017/jog.2016.28

530 Llorens, M.-G., Bons, P. D., Griera, A., Gomez-Rivas, E. and Evans, L.A., 2013. Single layer
531 folding in simple shear. Journal of Structural Geology, 50, 209-220.

532 Llorens, M-.G., Bons, P. D., Griera, A. and Gomez-Rivas, E., 2013. When do folds unfold
533 during progressive shear?. Geology, 41, 563-566.

534 Misra, S., and Burg, J.-P., 2012. Mechanics of kink-bands during torsion deformation of
535 muscovite aggregate. Tectonophysics, 548-549, doi:10.1016/j.tecto.2012.04.014.

536 Montagnat, M., Castelnau, O., Bons, P. D., Faria, S. H., Gagliardini, O., Gillet-Chaulet, F.,
537 Grennerat, F., Griera, A., Lebensohn, R. A., Moulinec, H., Roessiger, J., and Suquet, P.,
538 2014a. Multiscale modeling of ice deformation behavior. Journal of Structural Geology,
539 61, 78-108. doi:10.1016/j.jsg.2013.05.002.

540 Montagnat, M., Azuma, N., Dahl-Jensen, D., Eichler, J., Fujita, S., Gillet-Chaulet, F.,
541 Kipfstuhl, S., Samyn, D., Svensson, A. and Weikusat, I., 2014b. Fabric along the
542 NEEM ice core, Greenland, and its comparison with GRIP and NGRIP ice cores. The
543 Cryosphere, 8, 1129-1138, doi:10.5194/tc-8-1129-2014.

544 Nasello, O. B., Di Prinzio C. L. and Guzman, P. G., 2005. Temperature dependence of "pure"
545 ice grain boundary mobility. Acta Materialia, 53 (18), 4863-4869.
546 doi:10.1016/j.actamat.2005.06.022.

547 NEEM Community Members, 2013. Eemian interglacial reconstructed from a Greenland
548 folded ice core. Nature, 493, doi:10.1038/nature11789.

549 Paterson, W. S. B., 1991. Why ice-age ice is sometimes soft. Cold Regions Science and
550 Technology, 20(1), 75-98.

551 Peternell, M., Russell-Head, D. S., and Wilson, C. J. L., 2010. A technique for recording
552 polycrystalline structure and orientation during in situ deformation cycles of rock
553 analogues using an automated fabric analyser. Journal of Microscopy, 242(2), 181-188,
554 doi: 10.1111/j.1365-2818.2010.03456.x.

555 Quinquis, H., Audren, C., Brun, J.P., and Cobbold, P., 1978. Intensive progressive shear in
556 Ile de Groix blueschists and compatibility with subduction or obduction. Nature 274,
557 43-45.

558 Ramsay, J.G., and Huber, M., 1987. The Techniques of Modern Structural Geology. Volume
559 2: Folds and Fractures, Academic Press, London.

560 Rasmussen, S. O., Abbott, P. M., Blunier, T., Bourne, A.J., Brook, E., Buchardt, S. L.,
561 Buizert, C., Chappellaz, J., Clausen, H. B., Cook, E., Dahl-Jensen, D., Davies, S. M.,
562 Guillevic, M., Kipfstuhl, S., Laepple, T., Seierstad, I. K., Severinghaus,
563 J. P., Steffensen, J.P ., Stowasser, S., Svensson, S., Vallelonga, P., Vinther, B. M.,
564 Wilhelms, F. and Winstrup, M., 2013. A first chronology for the North Greenland
565 Eemian Ice Drilling (NEEM) ice core. Clim. Past, 9, 2713-2730, doi:10.5194/cp-9-
566 2713-2013.

567 Roessiger, J., Bons, P. D., Griera, A., Jessell, M. W., Evans, L. Montagnat, M., Kipfstuhl, S.,
568 Faria, S. H., and Weikusat, I., 2011. Competition between grain growth and grain size
569 reduction in polar ice. Journal of Glaciology 57, 942-948. doi:
570 10.3189/002214311798043690.

571 Roessiger, J., Bons, P. D., and Faria, S. H., 2014. Influence of bubbles on grain growth in ice.
572 Journal of Structural Geology. 61, 123-132. doi:10.1016/j.jsg.2012.11.00.

573 Russell-Head, D.S., and Wilson, C. J. L., 2001. Automated fabric analyser system for quartz
574 and ice. Geological Society of Australia, Abstracts, 64, 159.

575 Samyn, D., Weikusat, I., Svensson, A., Azuma, N., Montagnat, N. and Kipfstuhl, S., 2011.
576 Micro-structure of the NEEM deep ice core: towards quantifying stratigraphic
577 disturbances. Geophysical Research Abstracts, 13, EGU2011-12563-1, EGU General
578 Assembly 2011, http://meetingorganizer.copernicus.org/EGU2011/EGU2011-12563-
579 1.pdf.

580 Schulson, E. M., and Duval, P., 2009. Creep and fracture of ice (p. 432). Cambridge:
581 Cambridge University Press.

582 Svensson, A., Wedel Nielsen, S., Kipfstuhl, S., Johnsen, J., Steffensen, J. P., Bigler, M., Ruth,
583 U. and Röthlisberger, R., 2005. Visual Stratigraphy of the North Greenland Ice Core
584 Project (NorthGRIP) ice core during the last glacial period. J. Geophys. Res, 110,
585 D02108, doi:10.1029/2004JD005134.

586 Tanner, P. W. G., 1989 The flexural slip mechanism. J. Structural Geology, 11, 635-655.
587 doi:10.1016/0191-8141(89)90001-1.

588 Thorsteinsson, T., 1996. Textures and fabrics in the GRIP ice core, in relation to climate
589 history and ice deformation (Thesis). Berichte zur Polarforschung, 205, AWI
590 Bremerhaven.

591 Thorsteinsson, T., and Waddington, E. D., 2002. Folding in strongly anisotropic layers near
592 ice-sheet centers. Annals of Glaciology, 35, 480-486.

593 Thorsteinsson, T., 2002. Fabric development with nearest-neighbour interaction and dynamic
594 recrystallization. Journal of Geophysical Research 107 (B1), 2014.

595 Waddington, E. D, Bolzan, J. F. and Alley, R. B., 2001. Potential for stratigraphic folding
596 near ice-sheet centres. J. Glac., 47(159), 639-648.

597 WAIS Divide Project Members, 2013. Onset of deglacial warming in West Antarctica driven
598 by local orbital forcing. Nature, 500(7463), 440-444, doi: 10.1038/nature12376.

599 Wang, Y., Thorsteinsson, T., Kipfstuhl, J., Miller, H., Dahl-Jensen, D., and Shoji, H., 2006. A
600 vertical girdle fabric in the NorthGRIP deep ice core, North Greenland. Annals of
601 Glaciology, 35, 515-520.

602 Weikusat, I., and Kipfstuhl, J., 2010. Crystal c-axes (fabric) of ice core samples collected
603 from the NEEM ice core. Alfred Wegener Institute, Helmholtz Center for Polar and
604 Marine Research, Bremerhaven, Unpublished dataset #744004.

605 Williams, P. F., and Price, G.P. , 1990. Origin of kinkbands and shear-band cleavage in shear
606 zones: an experimental study. Journal of structural Geology, 12 (2), 145-164,
607 doi:10.1016/0191-8141(90)90001-F

608 Wilson, C. J. L., Burg, J. P. and Mitchell, J. C., 1986. The origin of kinks in polycrystalline
609 ice. Tectonophysics, 127, 27-48.

610 Wilson, C. J. L., and Russell-Head, H. M. S., 2003. The application of an automated fabric
611 analyser system to the textural evolution of folded ice layers in shear zones. Annals of
612 Glaciology, 37, 7-17.
613

Figure Captions

Figure 1: Visual stratigraphy overview. Linescan images of different depths. A Gauss filter was applied to images shown in panel a, d, e, f, g, and h to enhance the visibility of the layers. Red lines indicate fractures. Blue squares and associated figure codes indicate location of enlargements shown in figure 2. The 1.10 m line at the right indicates the scaling of the images and is also the typical length of a recovered core section.

Figure 2: Close-ups from the overview figure 1. (a) Undisturbed layering. (b) Angular z fold consistent throughout layering. Green dashed line indicates a layer discussed in section 3.1 (c) Different generation of folds. The dashed lines indicate features discussed in section 3.1 (d) Strongly disturbed layer significantly thickened. (e) Strongly disturbed layering with different generations of folds.

Figure 3: Comparison of fabric data and visual stratigraphy in detail, Bag 3276, approximate depth 1803 m. (a) fabric data in a vertical section, (b) linescan image in a vertical section, (c) stereoplot of c-axes orientations (horizontal plane).

Figure 4: (a) Close-up of kink band grains at approximately 1803 m depth (bag 3276). Inset shows the colour code for c-axes orientation (b) subgrain structures (blue) visible on LASM (Large Area Scanning Macroscope) data. Black lines indicate grain boundaries; the red outlines highlight the kink band grains.

Figure 5: Linescan images from the same sample as shown in fig. 3 from three focal depths with one highlighted layer (a) close to the surface, (b) in the centre of the core section, (c) close to the lower surface. (d) Sketch of the core sections, the upper part represents the physical properties sample, from which the thin sections are prepared. (e) Change of shape of the highlighted layer for the different foci.

Figure 6: Comparison of fabric data and visual stratigraphy in detail, Bag 3596, approximate depth 1977.8 m. (a) fabric data in a vertical section, (b) linescan image, in a vertical section (c) stereoplot of c-axes orientations (horizontal plane).

Figure 7: Comparison of entire 55 cm core sections (full bags) of linescan (a, d) and fabric data (b,c).

Figure 8: ELLE model results for the simple shear experiment. Panels (a), (b) and (c) show c-axes orientations for shear strains of γ=1, γ=2 and γ=3. Panels (d), (e) and (f) show the

644 distortion of the passive grid marker. Panels (g), (h) and (i) show the equivalent von Mises
645 strain-rate field.

646 **Figure 9:** Basic folding mechanisms discussed in the text. (a) Passive folds form by shearing
647 of disturbances in layering, without an active mechanical influence of that layering. Fold
648 geometry is that of similar folds. (b) Buckle folds form by shortening of alternating strong and
649 weak layers, in which the strong layers buckle and weak material flows into fold hinges. Fold
650 geometry is that of parallel folds. (c) Kink bands form in case of strong intrinsic anisotropy,
651 but do not require viscosity contrasts between layers.

652 **Figure 10:** Comparison of the onset of visible folding in ice cores with published visual
653 stratigraphy. The red line indicates single maximum fabric, the black line indicates onset of
654 folding, the dashed black line indicated the lower third of the ice core. Data from
655 Thorsteinsson, 1996 (GRIP), Alley et al., 1997; Gow et al., 1997 (GISP2), Svensson et al.,
656 2005; Wang et al., 2006 (North GRIP), Faria et al., 2010 (EDML), Fitzpatrick et al., 2014
657 (WAIS).
658

659

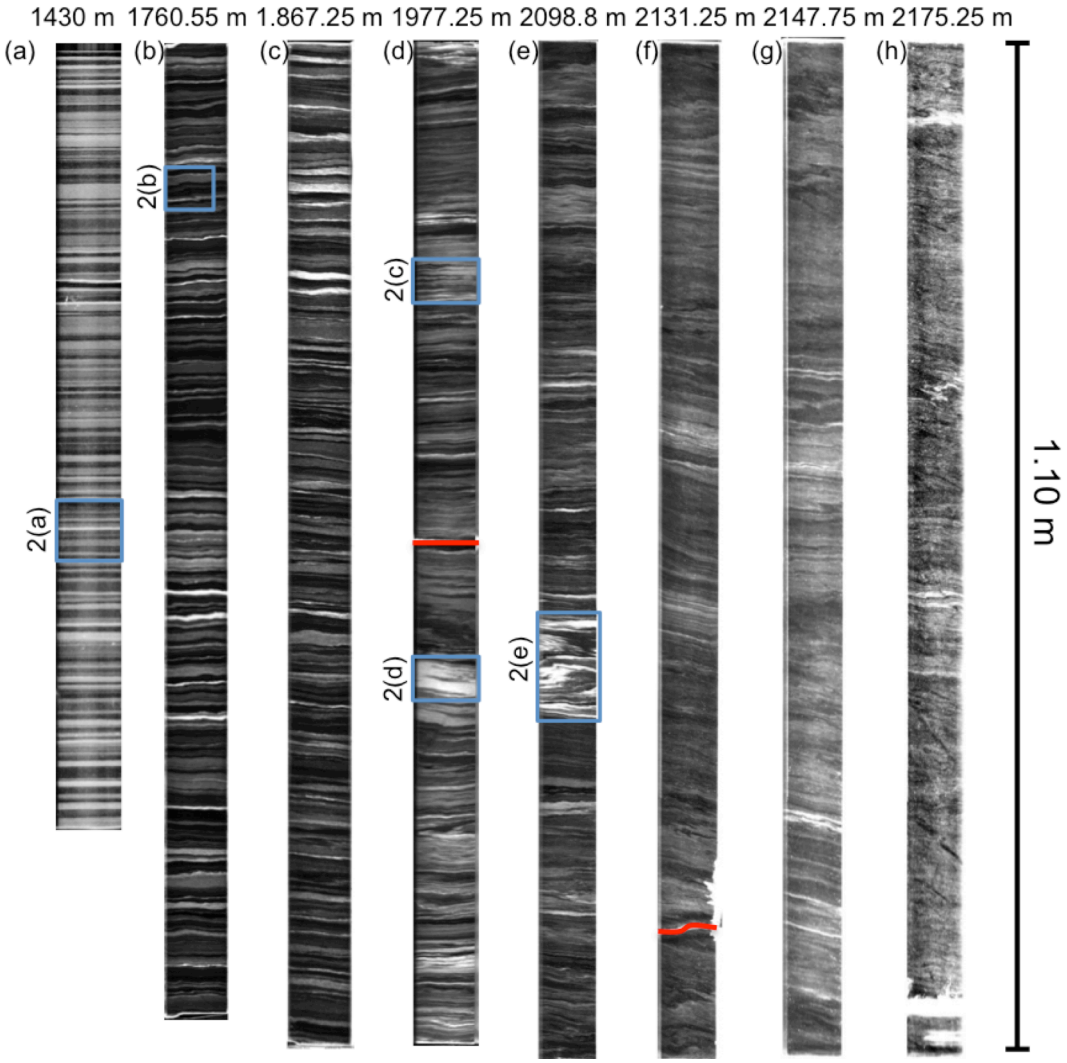

660

661 Figure 1

662

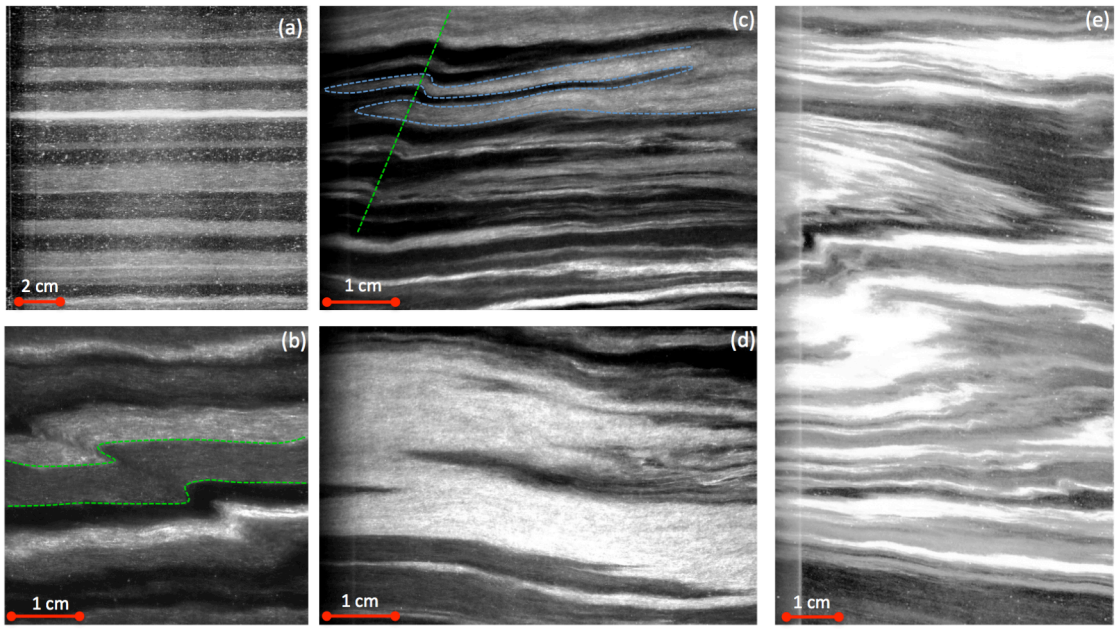

663
664 Figure 2
665

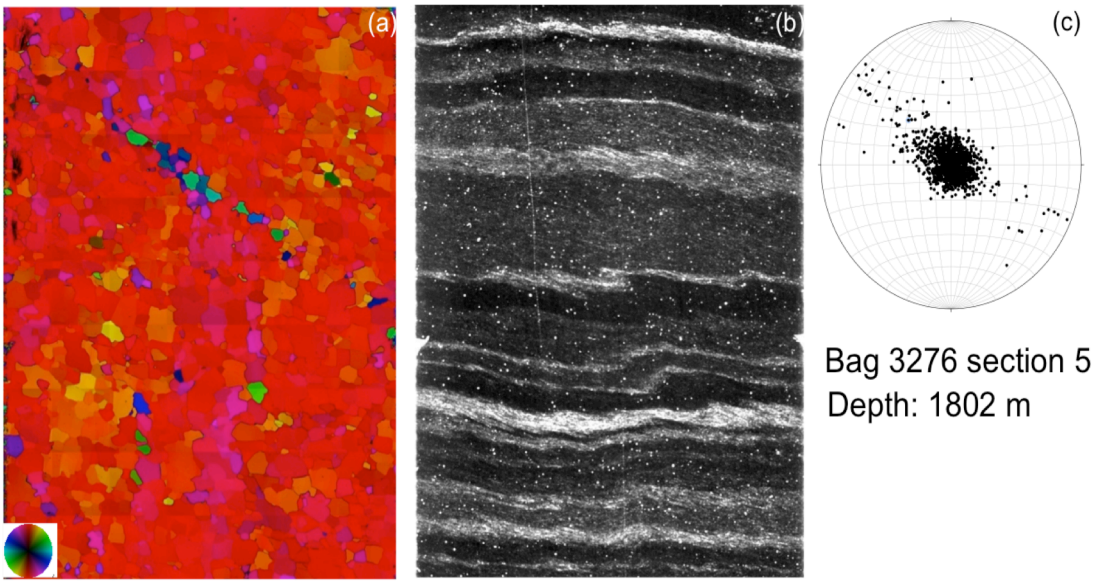

Figure 3

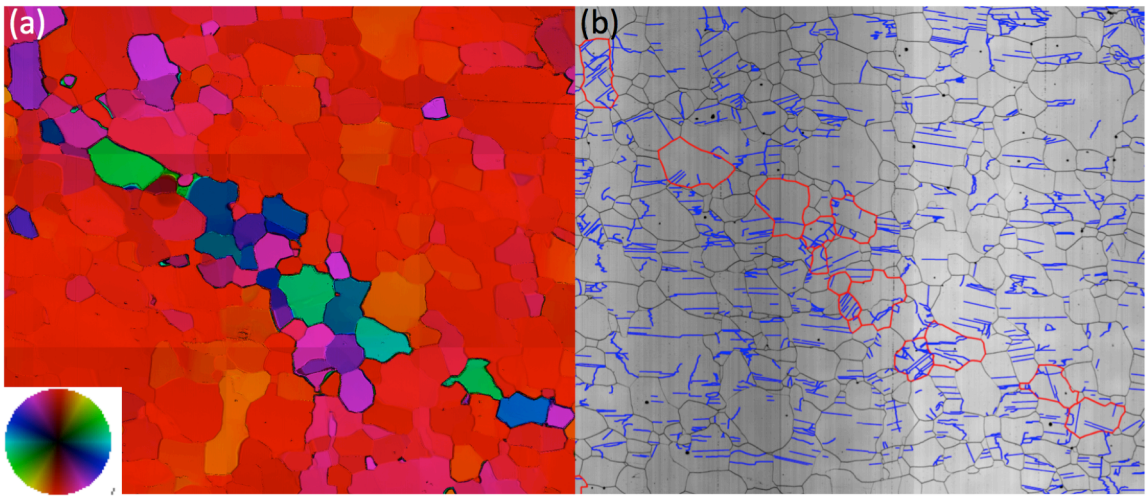

669
670 Figure 4
671

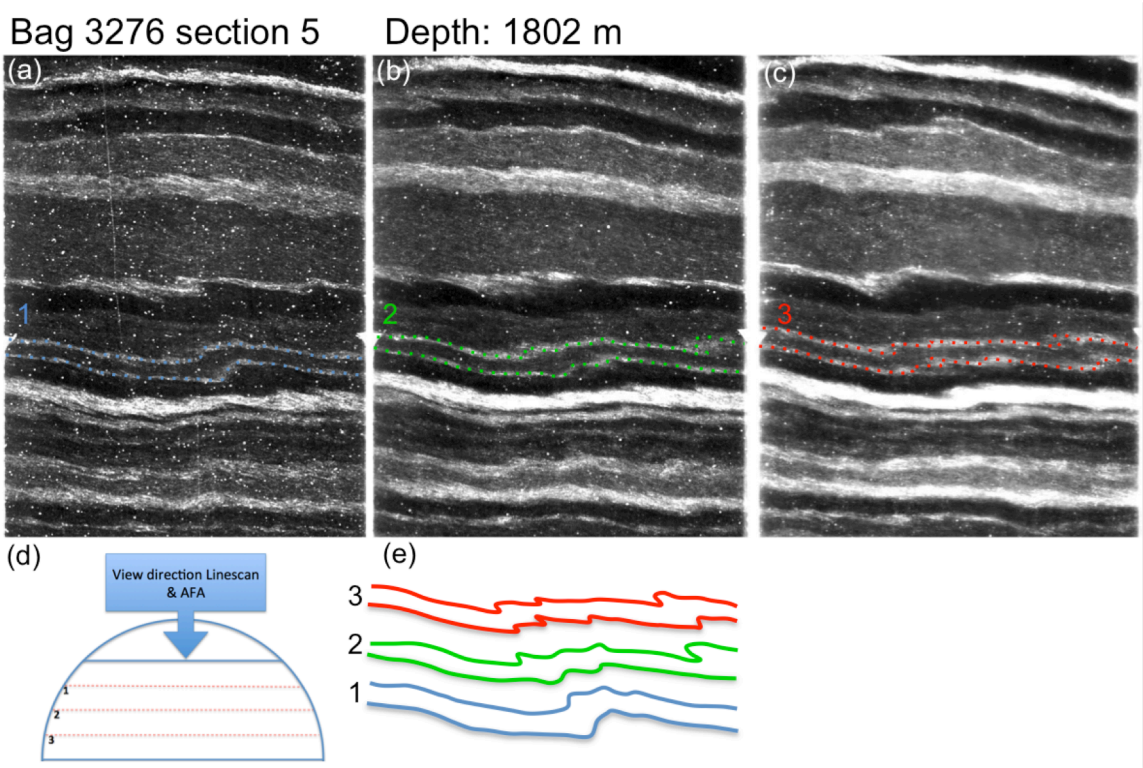

672 Figure 5
673

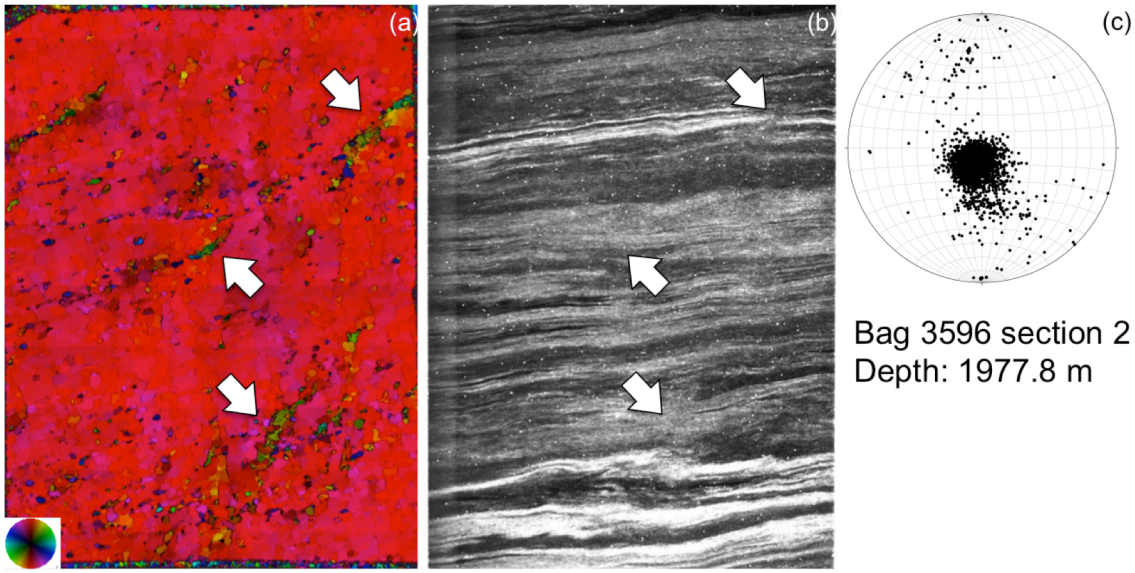

674 Figure 6
675

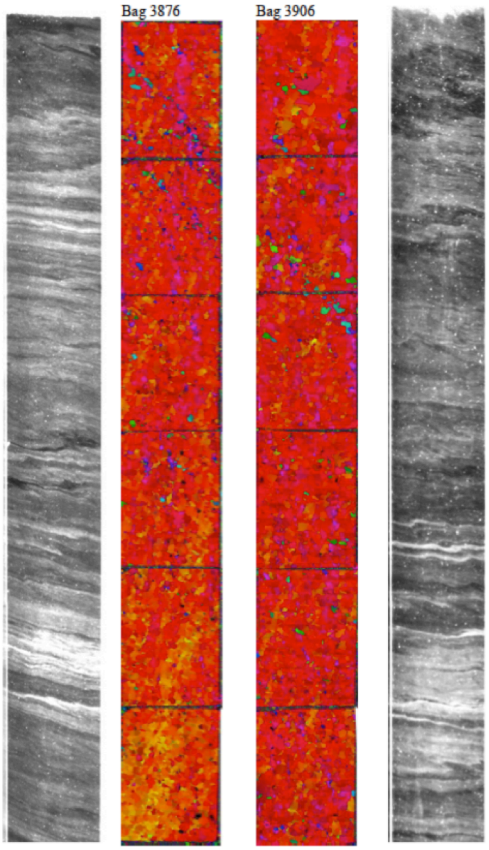

676 Figure 7
677

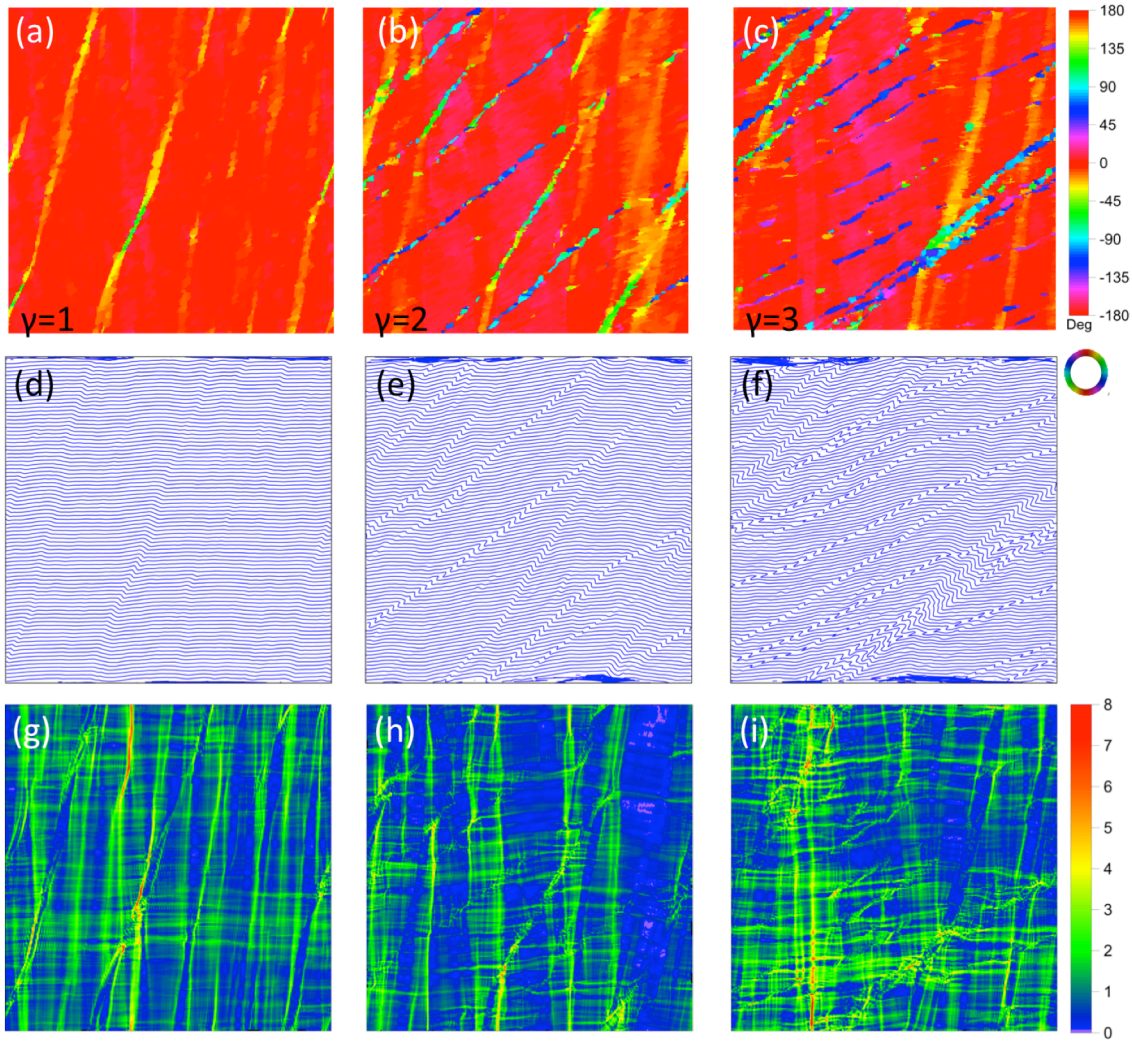

678 Figure 8
679

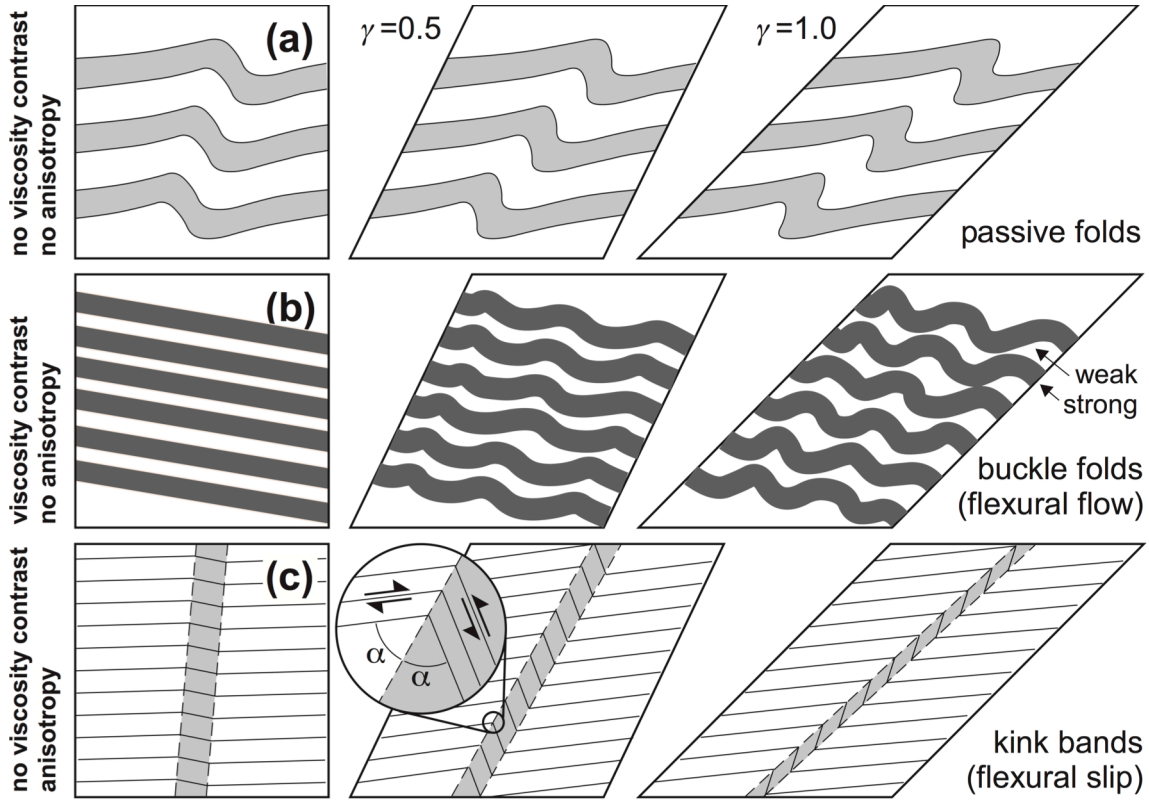

680 Figure 9
681

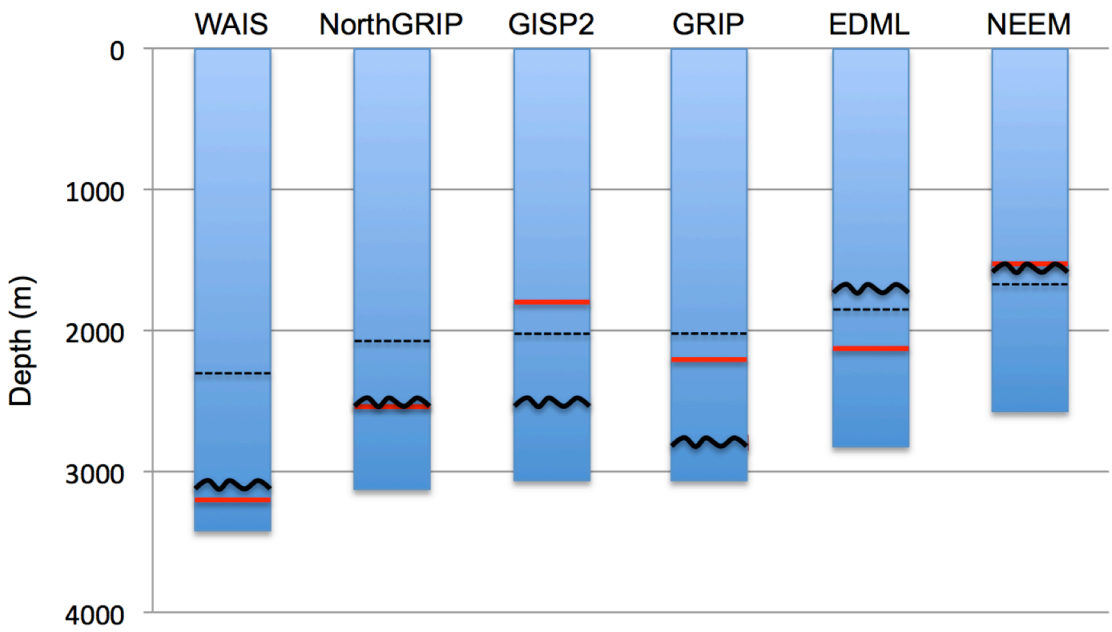

682 Figure 10
683
684
685